ACS Catalysis

Research Article

pubs.acs.org/acscatalysis

# Hierarchical Nanostructured 3D Flowerlike $BiOCl_xBr_{1-x}$ Semiconductors with Exceptional Visible Light Photocatalytic Activity

Hani Gnayem and Yoel Sasson*

Casali Institute of Applied Chemistry, Institute of Chemistry, The Hebrew University of Jerusalem, Jerusalem 91904, Israel

Supporting Information

**ABSTRACT:** With careful rational optimization and substantial simplification of the syntheses of the recently reported alloys $BiO(Cl_xBr_{1-x})$, we fabricated, via a very simple procedure and at room temperature, a unique visible-light-driven photocatalyst with excellent activity. The alloy $BiOCl_{0.875}Br_{0.125}$ totally decomposed 15 mg/L aqueous Rhodamine B solution within 120 s upon irradiation with visible light ($\lambda$ > 422 nm). The transparent substrate acetophenone was also swiftly destroyed under the above conditions. The catalyst maintained partial activity even after switching off the light source. Initial mechanistic studies clearly suggest that the mode of action of these materials is fundamentally different from previously reported photocatalytic mechanisms. Evidently, the putative molecular mechanism does not engage dye photosensitization or oxygen radicals.

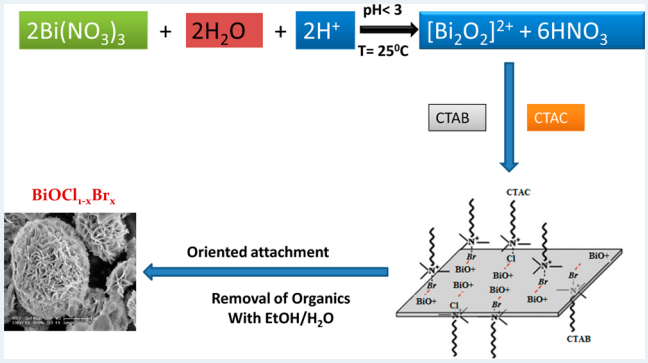


**KEYWORDS:** *bismuth mixed oxyhalides, visible light photocatalyst, Rhodamine B decomposition, acetophenone decomposition*

## INTRODUCTION

With the ever-increasing interest in environmentally friendly processes and products and in renewable energy sources, photocatalysis has recently attracted a great deal of attention,[1] with particular focus on water and air purification[2−4] and disinfection.[5] $TiO_2$ is by far the leading commercial photocatalyst characterized by high activity, simple processing, notable stability, and low cost.[6] Unfortunately, its band gap is too wide for efficient utilization of visible irradiation. Aiming at developing visible-light-driven photocatalysts, research in numerous laboratories has focused on doping $TiO_2$ with various dopants,[7−9] using $TiO_2$−carbon composites,[10] or searching for non-$TiO_2$ catalysts, typically heavy metal compounds.[11] Nonetheless, adequately stable and practically usable visible light photocatalysts have not yet been fully realized.

Following the discovery of bismuth-based ternary metal oxide photocatalysts, such as $Bi_2WO_6$,[12] bismuth oxyhalides (BiOXs; X = F,[13] Cl,[14−16] Br,[17−19] I[20]) have lately been found to exhibit remarkable photocatalytic activity under UV and visible light irradiation.[21] Alloyed compounds containing more than one type of halogen,[22] such as $BiOI_xCl_{1-x}$[23] and $BiOBr_xI_{1-x}$,[24] were noticed to be even more effective than the corresponding pure forms. The structure of these oxyhalides comprises a layer of $[Bi_2O_2]^{2+}$ slabs interleaved by double slabs of halogen atoms.[25] The unique catalytic properties of these materials were attributed to the high dipole moment (value above 2.00 D) within most of the BiOX crystals, the indirect band gaps, high redox potential of the holes, low electron−hole recombination rates, and the easy formation of O vacancies.[22]

We[26] and others[27] have recently reported a new family of $BiO(Cl_xBr_{1-x})$ compounds synthesized via a hydrothermal method. These alloys exhibited unique photocatalytic activity under visible light in degradation of Rhodamine B and acetophenone and in the photoxidation of iodide ion. The material with X = 0.5 was shown to be three times more active than Degussa's P25 in photodegradation of Rhodamine B under visible light irradiation.[26]

We have now observed that with the right selection of the reagents and with optimizing the synthetic protocol for the fabrication of $BiO(Cl_xBr_{1-x})$ alloys, far more potent photocatalytic materials with unique morphologies are obtained. These hierarchiral 3D nanostructured compounds exhibited visible-light-induced photocatalytic activity that is considerably higher than $TiO_2$ and is substantially superior (in terms of RhB decomposition rate) to previously reported visible light photocatalysts. In addition, the synthetic protocol of these alloys could be dramatically simplified. Hydrothermal methods are not necessary, and the complete procedure is accomplished within minutes under ambient conditions.

**Received:** August 2, 2012
**Revised:** December 31, 2012
**Published:** January 2, 2013

  

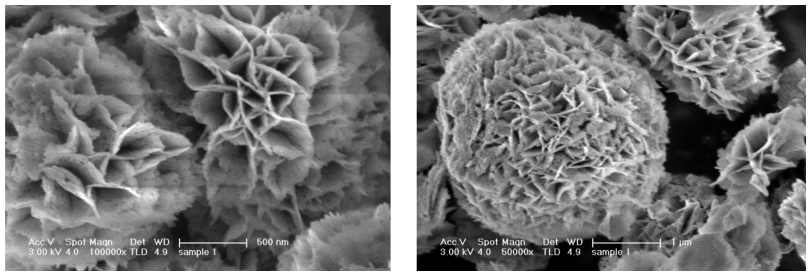

**Figure 1.** SEM images of the as-prepared $BiOCl_{0.875}Br_{0.125}$ using CTAB and CTAC as halide sources.

## RESULTS AND DISCUSSION

**Catalysts Preparation and Characterization.** Reassessing our previous hydrothermal synthetic protocol[26] and evaluating the solvothermal synthesis of flowerlike BiOBr microspheres reported by Huo and co-workers,[28] we identified five key crucial experimental variables for the modified syntheses of the novel upgraded $BiOCl_xBr_{1-x}$ photocatalytic materials reported herein: (1) the nature of the solvent used in the preparation, (2) the pH of the reaction mixture, (3) the reaction temperature and time, (4) the type of the reagents supplying the bromide and chloride anions, and (5) the $Cl^-/Br^-$ ratio in the final product (which is evidently identical to the molar ratio used in the starting materials).

The ordinary source for bismuth cation in the preparation of BiOXs is bismuth nitrate (probably due to availability and cost). This salt is inadequately soluble in water, and thus, its reaction with aqueous base (typically ammonium hydroxide) is not homogeneous in nature, even when conducted at high temperature for a long period of time in an autoclave (130 °C for 14 h according to our previously reported conditions[26]). As a result, the reaction usually does not go to completion. Neutral conditions, using alcohols or diols as solvents, also require long periods of heating under pressure at high temperature (160 °C for 12 h).[28,29] We have now found that the key intermediate species $[Bi_2O_2]^{2+}$ is swiftly formed under *acidic aqueous conditions* where bismuth nitrate is completely soluble. Consequently, the application of, for example, acetic acid as cosolvent facilitates an instant reaction between $Bi^{3+}$, water, and the halide anions at room temperature, yielding the desired bismuth oxyhalide products as an easily separable precipitate. (eqs 1,2)

$$2Bi(NO_3)_3 + 2H_2O + 2H^+ \rightarrow [Bi_2O_2]^{2+} + 6HNO_3 \quad (1)$$

$$[Bi_2O_2]^{2+} + x2Cl^- + (1 - x)2Br^- \rightarrow 2BiOCl_xBr_{1-x} \quad (2)$$

Interestingly, in a recent related work, Jiang and associates have demonstrated that modifying the pH of a similar reaction mixture critically affects the nature of the facet of the BiOCl single crystalline nanosheets formed, leading to different photocatalytic properties. The {010} facet was obtained in the presence of NaOH, and the {001} facet was prepared under neutral conditions.[30,31] These two materials exhibited different photocatalytic activities.

The reaction between halide anions and a homogeneous solution of bismuth nitrate in acetic acid−water (0.5−10:1 v/v) mixture at room temperature is swift, and a precipitation is obtained instantly. The latter is straightforwardly filtered, thoroughly washed for removal of organics, and dried under ambient conditions and can then be *directly used* as a photocatalyst.

The nature of the halide reagents providing the chloride and bromide anions for the composite catalyst is critical for determining the morphology and, consequently, the catalytic capacity of the product. We discovered that surface-active quaternary ammonium salt, such as cetyltrimethylammonium halides (CTAC and CTAB), afforded the best results. These reagents evidently have a dual function in this procedure. They simultaneously serve as bromide and chloride suppliers and also as structure-directing agents. (This was recently also shown in the synthesis of BiOBr using CTAB as a bromide source.[28,32]) The instantly formed crystalline product is composed of a 3D hierarchical, flowerlike, microsphere 1.5−3 $\mu$m in diameter (see SEM image in Figure 1).

Conversely, when a mixture of NaCl/KBr was used as a halides source, under otherwise identical conditions, the particles obtained were characterized as having a flakelike morphology, as shown in Figure 2. These materials, which have

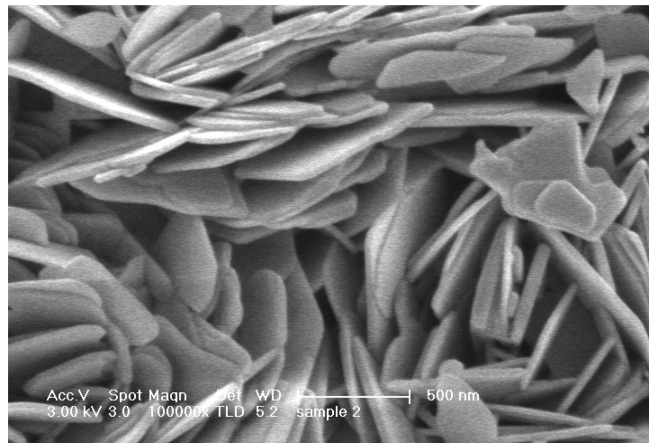


**Figure 2.** SEM image of the as-prepared $BiOCl_{0.875}Br_{0.125}$ using NaCl and KBr as halide sources.

indistinguishable chemical composition, $BiOCl_{0.875}Br_{0.125}$, were found to be far less active as visible light photocatalysts (see below). The critical role of the morphology of BiOCl microcrystals in determining the photoactivity was recently demonstrated also by Zhang and associates.[33] The unique photochemical properties of flowerlike BiOBr microspheres were explored and scrutinized by Huo et al.[28]

The phase purity of the as-prepared $BiOCl_xBr_{1-x}$ alloys was determined by XRD measurements, which confirmed that the Cl/Br ratio in the final product is accurately determined by the proportion of the halides sources utilized in the starting mixture. Figure 3 displays the XRD diffraction pattern of


dx.doi.org/10.1021/cs3005133 | ACS Catal. 2013, 3, 186−191

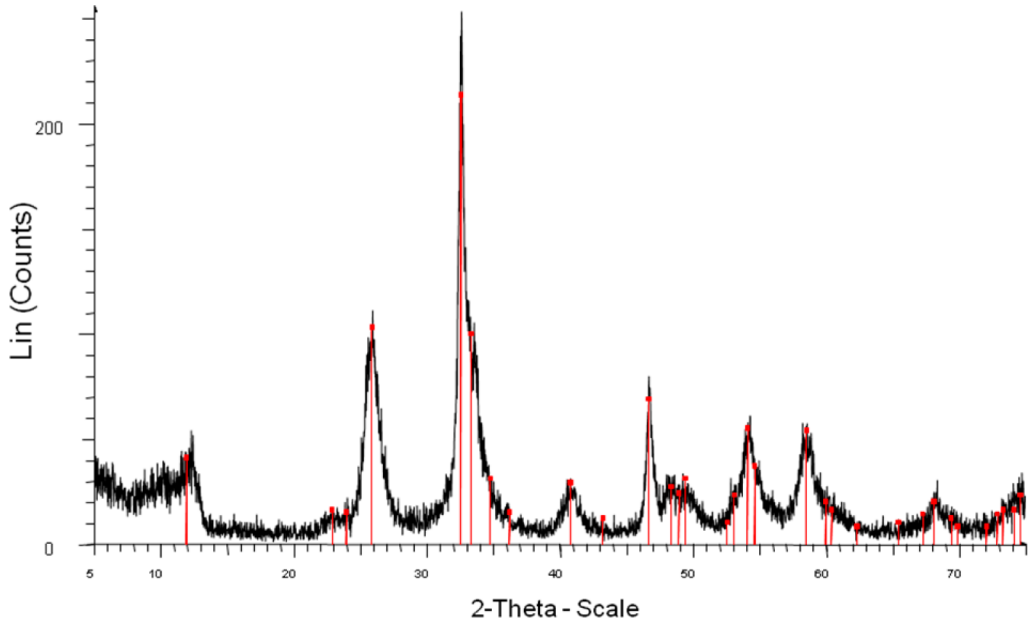


**Figure 3.** XRD diffraction pattern of $BiOCl_{0.875}Br_{0.125}$.

$BiOCl_{0.875}Br_{0.125}$. The diffraction patterns of other $BiOCl_xBr_{1-x}$ alloys prepared in this study are displayed in Figures S1−S3 in the Supporting Information.

Using diffuse reflectance spectroscopy, we have calculated the band gap energy of some of the above alloys. Thus, for $BiOCl_{0.875}Br_{0.125}$, we obtained 2.94 eV; for $BiOCl_{0.75}Br_{0.25}$, 2.81 eV; for $BiOCl_{0.67}Br_{0.33}$, 2.77 eV; and for $BiOCl_{0.5}Br_{0.5}$, 2.68 eV. For the pure BiOCl, we measured $E_g$ of 3.18 eV, and for pure BiOBr, 2.53 eV. For more details, see Table S1 in the Supporting Information. See also our previous report.[26] The Brunauer−Emmett−Teller (BET) surface area, particle size, and the $\zeta$ potential measured for the above $BiOCl_xBr_{1-x}$ compounds are present in Table 1.

**Table 1. BET Surface Area, Particle Size and $\zeta$ Potential at pH = 7 of the As-Prepared $BiOCl_xBr_{1-x}$ Alloys**

| $X$ value | BET ($m^2$/g) | particle size ($\mu$m) | $\zeta$ potential (mV) |
|---|---|---|---|
| 0 | 8.86 | 5.78 | −48.4 |
| 0.5 | 6.00 | 11.28 | −30.4 |
| 0.67 | 16.84 | 4.96 | −23.6 |
| 0.73 | 15.62 | 2.86 | −16.3 |
| 0.80 | 25.75 | 2.62 | −16.1 |
| 0.875 | 26.87 | 1.98 | −12.5 |
| 1.0 | 12.54 | 3.67 | −14.9 |

The $\zeta$ potential (ZP) was found to be strongly pH-dependent. This is shown in Figure S6 in the Supporting Information. At low pH, the ZP of $BiOCl_{0.875}Br_{0.125}$ is positive, but above pH = 4, it is negative and linearly decreasing until pH = 14. The ZP of pure BiOBr and BiOCl was recently measured by Chang and associates.[34] These authors observed the same trend in the effect of pH on the ZP of these materials; however, their values are different.

**Adsorption and Photocatalytic Activity Measurements Using RhB As a Substrate.** Adsorption of the substrate to the photocatalyst surface is considered a critical step in photo-induced degradation processes.[34,35] We have measured the adsorption of RhB to the $BiOCl_xBr_{1-x}$ alloys under dark conditions. Results are presented in Table 2 (% of RhB adsorbed in 1 h under the given settings).

**Table 2. Adsorption and Photocatalytic Decomposition of RhB in the Presence of $BiOCl_xBr_{1-x}$**

| formula | % adsorption of RhB in the dark after 1 h | RhB decomposition under visible light at $t_{1/2}$ (s) |
|---|---|---|
| BiOBr | 14 | 810 |
| $BiOCl_{0.50}Br_{0.50}$ | 6 | 540 |
| $BiOCl_{0.67}Br_{0.33}$ | 4 | 60 |
| $BiOCl_{0.75}Br_{0.25}$ | 3 | 24 |
| $BiOCl_{0.80}Br_{0.20}$ | 3 | 23 |
| $BiOCl_{0.875}Br_{0.125}$[a] | 1 | 17 |
| $BiOCl_{0.875}Br_{0.125}$[b] | 19 | 630 |
| BiOCl | 8 | 690 |

[a]CTAB and CTAC were used as halide sources. [b]NaCl and KBr were used as halide sources.

The same table also displays the measured photocatalytic activity of the $BiOCl_xBr_{1-x}$ alloys. This was calculated by monitoring the degradation of aqueous Rhodamine B (RhB, 15 mg/L aqueous solution) under visible light ($\lambda \geq 422$ nm) irradiation (see the Experimental Section for details). The photocatalytic activity is expressed as the time needed for 50% decomposition of 15 mg/L aqueous solution of RhB measured by UV absorption. Complete conversion is eventually attained in all these experiments. We could not fit the kinetic profile of these reactions (see Figure 4) to a first-order rate law, which was suggested in previous studies.[28]

It can be concluded that the highest visible light photocatalytic performance is observed with $BiOCl_xBr_{1-x}$ alloy, where $x$ is 0.875. As described above, this composite is straightforwardly prepared by controlling the initial molar ratio of CTAC/CTAB in the preparation protocol. Remarkably, the observed catalytic activity increases with *decreasing* degree of adsorption: the more potent photocatalyst adsorbs hardly any amount of RhB (1%). This could be rationalized by the masking effect of the adsorbed substrate that obstructs the transfer of light to the


dx.doi.org/10.1021/cs3005133 | ACS Catal. 2013, 3, 186−191

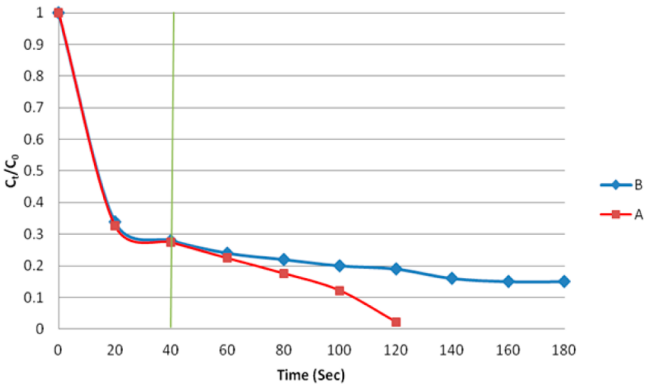


**Figure 4.** (A) Time-resolved degradation of RhB in the presence of $BiOCl_{0.875}Br_{0.125}$ under irradiation of visible light (422−740 nm). (B) Same as above, but the light was turned off after 40 s.

catalyst surface, thus impeding the photoactivation in experiments in which a high degree of adsorption is observed.

Using $BiOCl_{0.875}Br_{0.125}$ as a catalyst, we measured complete destruction of RhB under the above conditions in 120 s. The destruction is absolute, as can be seen in Figure S7 in the Supporting Information. The kinetic profile of the degradation process is shown in Figure 4 and in Figure S4 in the Supporting Information. Figure S5 displays the slower RhB decomposition using $BiOCl_{0.50}Br_{0.50}$ as catalyst under identical conditions. The photocatalytic activity of $BiOCl_{0.875}Br_{0.125}$ was maintained for 10 consecutive runs in which a fresh batch of RhB was added each time after the previous batch was fully consumed within 120 s. Note that in the absence of a catalyst, the decomposition of RhB under visible light is negligible. Interestingly, turning the light source off in the course of the process (after 40 s) did not terminate the decomposition progression. Slow decomposition was monitored for more than additional 120 s. This is also shown in Figure 4.

When a domestic 11 W PL bulb (placed 10 cm away from the reaction mixture) was used as the light source, the same 15 mg/L RhB solution totally decomposed within 10 min in the presence of $BiOCl_{0.875}Br_{0.125}$. We confirmed that the microscopic appearance of the catalyst particles and its XRD pattern did not change after the 10 consecutive runs described above. Moreover, used $BiOCl_{0.875}Br_{0.125}$ photocatalyst, which was kept under ambient conditions for 4 weeks, was found to retain its original activity. In addition, heating the latter alloy at 400 °C for 4 h did not affect its room temperature photocatalytic performance. To the best of our knowledge, the above rate of RhB destruction under visible light irradiation is the highest of any previously reported photocatalyst[36]

**Photocatalytic Destruction of Acetophenone Using $BiOCl_{0.875}Br_{0.125}$ under Visible Light.** The use of dyes as reference substrates in photocatalysis was rejected by several authors because of the possibility of dye sensitization.[37,38] Consequently, we have examined the photocatalytic decomposition of the visible-light-transparent molecule acetophenone (AP) in the presence of $BiOCl_{0.875}Br_{0.125}$. A 150 mg portion of catalyst was mixed with 200 mL of water containing 150 mg/L of AP under dark conditions for 90 min. Only 2% of the AP was found to adsorb to the catalyst surface during this time. Visible light ($\lambda \geq 422$ nm) was then applied, and the decomposition of AP was monitored by following the UV absorbance of samples taken from the reaction mixture (see Figure S8 in the Supporting Information). The kinetic profile of AP decomposition is shown in Figure 5. It is apparent that 93% of the initial AP molecules were destructed in 3 h of irradiation.

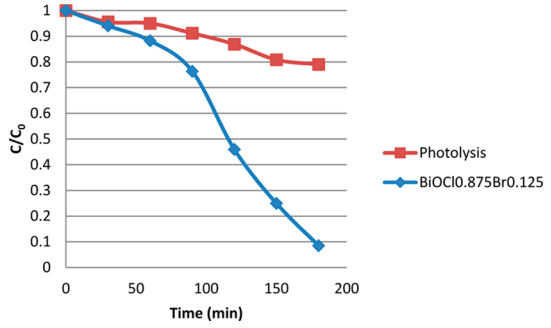


**Figure 5.** Time-resolved degradation of AP in the presence of $BiOCl_{0.875}Br_{0.125}$ under irradiation of visible light (422−740 nm).

AP is sensitive to noncatalytic photolysis. We have tested the photolysis of the above AP solution under visible light in the absence of a catalyst and found that 21% of the material decomposed within 3 h. We may safely conclude that the greater part (70%) of the decomposition process resulted from the photocatalysis.

**Mechanistic Studies.** In an attempt to identify the reactive intermediates in the RhB photocatalytic process, we examined the effect of common inhibitors on the RhB decomposition rate. We could not substantiate the presence of any of the expected reactive species, such as superoxide anion, hydroxyl radical, or photogenerated holes or electrons. Running the above experiment in the presence of benzoquinone (a superoxide trap[39,40]) or in the presence of terephthalic acid or *tert*-butyl alcohol (hydroxyl radical scavengers[41]) did not affect the rate of RhB decomposition. Addition of EDTA (a strong hole scavenger[42]) or $AgNO_3$ (an electron trap[28]) to the photodecomposition process also had no apparent effect on the reaction rate.

Another extraordinary feature of these catalytic alloys was observed when the photocatalysis was carried out under a pure oxygen atmosphere. It was realized that all the above composites were far less active in RhB decomposition under oxygen. On the other hand, under nitrogen atmosphere, the decomposition rates were slightly higher. The performance of $BiOCl_{0.875}Br_{0.125}$ in RhB decomposition under pure oxygen and under nitrogen is displayed in Figure 6. It is well-known that the presence of oxygen is critical in photochemical systems for the generation of superoxide anion radical.[37] If oxygen retards the photocatalysis and nitrogen enhances it, we may safely

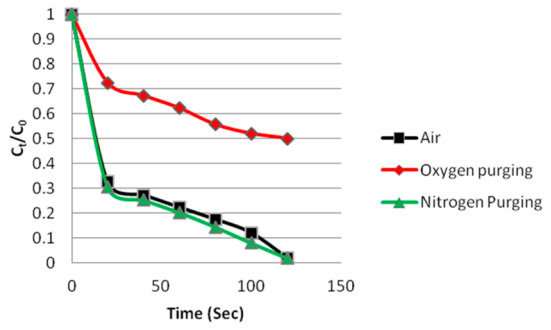


**Figure 6.** Degradation of RhB under visible light (422−740 nm) in the presence of $BiOCl_{0.875}Br_{0.125}$ under air, oxygen, and nitrogen.


dx.doi.org/10.1021/cs3005133 | *ACS Catal.* 2013, 3, 186−191

conclude that superoxide is not an intermediate in our process. Since superoxide is also the evident intermediate in dye photosensitization, we can also assert that the mechanism of our system is, most likely, not based on dye photosensitization.

It seems that the reactive species operating in this light-induced process are relatively long-living with half-life of seconds and that they are not confined to the photocatalyst's surface. We hypothesize that halide or oxyhalide radicals might be involved in the catalytic cycle. It could also be assumed that the formed internal electric fields between the $[Bi_2O_2]^{2+}$ positive slabs and the halogen anionic slabs induce efficient separation of photogenerated electron−hole pairs and thus improve the photocatalytic activity. We may also presume that the optical path length for light transporting through these flowerlike microstructures may be longer than that for the flakelike microplate samples. Thus, a longer optical path length and multireflections could increase the quantity of photogenerated electrons and holes available to participate in the photocatalytic decomposition process. A detailed mechanistic study of this system is now underway.

## CONCLUSIONS

The excellent photocatalytic activity of the nanostructured flowerlike mixed bismuth oxyhalides of the general formula $BiOCl_xBr_{1-x}$ is evidently strongly dependent on the fabrication protocol and the nature of the starting materials. The challenging molecular mechanism, which apparently does not consist of a dye sensitization step or oxygen radicals, is probably unlike any previously known photocatalytic process and is still to be deciphered.

## EXPERIMENTAL SECTION

**Materials.** All materials were purchased from Aldrich-Sigma and were used without further purification.

**Instruments.** XRD measurements were performed on a D8 Advance diffractometer (Bruker AXS, Karlsruhe, Germany) with a goniometer radius of 217.5 mm, Göbel Mirror parallel-beam optics, 2° Sollers slits, and 0.2 mm receiving slit. A low-background quartz sample holder was carefully filled with the powder samples. XRD patterns from 5° to 85° $2\theta$ were recorded at room temperature using Cu K$\alpha$ radiation ($\lambda$ = 0.154 18 nm) with the following measurement conditions: tube voltage of 40 kV, tube current of 40 mA, step scan mode with a step size 0.02° $2\theta$, and counting time of 1 s per step for preliminary study and 12 s per step for structural refinement. The instrumental broadening was determined using $LaB_6$ powder (NIST-660a).

Morphological observations were performed with a HRSEM high resolution scanning electron microscope Sirion (equipped with EDS LN2 detector, Oxford instruments, UK).

The particle size was measured using a Malvern Instruments Mastersizer 2000 particle size analyzer.

The $\zeta$ potential was measured using a Malvern Instruments Zetasizer Nano ZS.

The surface area and pore radius were determined by the N2 BET method (NOVA-1200e).

**Preparation of $BiOCl_{0.875}Br_{0.125}$.** Deionized water (85 mL), glacial acetic acid (45 mL), and bismuth nitrate (14.69 g, 30 mmol) are placed into a 250 mL flask and stirred at room temperature for 15 min until a clear, transparent solution is formed. Then CTAB (1.378 g dissolved in 10 mL of water, 3.5 mmol) and CTAC (8.48 g of 25 wt % aqueous solution, 26.5 mmol) are added to the above solution in one batch, and the mixture is stirred for an additional 30 min at room temperature. The precipitate thus formed is filtered and washed five times with ethanol (50 mL) and five times with water (200 mL) to remove the nonreactive organic species. The white solid is then dried (in air) and is ready for use. The weight of the solid collected was 10.5 g (94% yield)

The product exhibits an X-ray powder diffraction pattern having characteristic peaks at 12.04, 25.86, 32.56, 46.68, and 58.40 $2\theta$ (±0.05 $2\theta$). The average particle size was 1.98 $\mu$m; the surface area (BET), 26.87 $m^2/g$; and the pore radius, 24 Å.

**Adsorption and Photocatalytic Experiments.** Experiments were carried out in a 250 mL cylindrically shaped glass reactor at room temperature under air and at neutral pH. A suspension of 150 mg of catalyst in 200 mL of aqueous solution of RhB (15 mg/L) was magnetically stirred in the dark for 1 h. After filtration, the amount of RhB adsorbed was measured by UV absorption of the solution. The same procedure was used in the photocatalytic experiments. The mixture was irradiated by a 300W Xe arc lamp (Max-302, Asahi spectra). Power consumption of Max-302 was 500 VA.

For visible light experiments, a 422 nm cutoff filter was used. The light intensity was fixed at 70 $mW/cm^2$, and the reactor was placed 10 cm away from the light's source mirror. At specific time intervals, 5 mL samples were taken and centrifuged at 6000 rpm for 10 min to remove the photocatalyst particles. The concentration of the remnant RhB solution was assayed with a UV−vis spectrophotometer (Varian EL-03097225) by recording the variations of the absorption band maximum at $\lambda$ = 554 nm.

## ASSOCIATED CONTENT

### Supporting Information

Additional information as noted in text. This material is available free of charge via the Internet at http://pubs.acs.org.

## AUTHOR INFORMATION

### Corresponding Author

*Phone: +972 2658 4530. Fax: +972 2652 9626. E-mail: ysasson@huji.ac.il.

### Notes

The authors declare no competing financial interest.

## REFERENCES

(1) Kubacka, A.; Fernandez-Garcia, M.; Colon, G. *Chem. Rev.* **2012**, *112*, 1555−1614.
(2) Herrmann, J.-M. *Catal. Today* **1999**, *53*, 115−129.
(3) Kabra, K.; Chaudhary, R.; Sawhney, R. L. *Ind. Eng. Chem. Res.* **2004**, *43*, 7683−7696.
(4) Chan, S. H. S.; Wu, T. Y.; Juan, J. C.; Teh, C. Y. *J. Chem. Technol. Biotechnol.* **2011**, *86*, 1130−1158.
(5) Robertson, P. K. J.; Robertson, J. M. C.; Bahnemann, D. E. *J. Hazard. Mater.* **2012**, *211−212*, 161−71.
(6) Paz, Y. *Appl. Catal., B* **2010**, *99*, 448−460.
(7) Girish, K. S.; Gomathi, D. L. *J. Phys. Chem. B* **2011**, *115*, 13211−13241.
(8) Han, F.; Kambala, V. S. R.; Srinivasan, M.; Rajarathanm, D.; Naidu, R. *Appl. Catal., A* **2009**, *359*, 25−40.
(9) Hu, Y.; Cao, Y.; Wang, P.; Li, D.; Chen, W.; He, Y.; Fu, X.; Shao, Y.; Zheng, Y. *Appl. Catal., B* **2012**, *125*, 294−303.
(10) Di Paola, A.; Garcia-Lopez, E.; Marci, G.; Palmisano, L. *J. Hazard. Mater.* **2012**, *211−212*, 3−29.
(11) Hernandez-Alonso, M. D.; Frenso, F.; Suarez, S.; Coronado, J. M. *Energy Environ. Sci.* **2009**, *2*, 1231−1257.

(12) Zhang, L.; Zhu, Y. *Catal. Sci. Technol.* **2012**, *2*, 694−706.
(13) Su, W.; Wang, J.; Huang, Y.; Wang, W.; Wu, L.; Wang, X.; Liu, P. *Scr. Mater.* **2009**, *62*, 345−348.
(14) Zhang, K.-L.; Liu, C.-M.; Huang, F.-Q.; Zheng, C.; Wang, W.-D. *Appl. Catal., B* **2006**, *68*, 125−129.
(15) Pare, B.; Sarwan, B.; Jonnalagadda, S. B. *J. Mol. Struct.* **2012**, *1007*, 196−202.
(16) Ye, L.-Q.; Deng, K.-J.; Xu, F.; Tian, L.-H.; Peng, T.-Y.; Zan, L. *Phys. Chem. Chem. Phys.* **2012**, *14*, 82−85.
(17) Zhang, X.; Hi, Z. H.; Jia, F. L.; Zhang, L. Z. *J. Phys. Chem. C* **2008**, *112*, 747−753.
(18) Zhang, J.; Shi, F. J.; Lin, J.; Chen, D. F.; Gao, J. M.; Huang, Z. X.; Ding, X. X.; Tang, C. C. *Chem. Mater.* **2008**, *20*, 2937−2941.
(19) Cheng, H.; Huang, B.; Wang, Z.; Qin, X.; Zhang, X.; Dai, Y. *Chem.—Eur. J.* **2011**, *17*, 8039−8043.
(20) Shi, X.; Chen, X.; Chen, X.; Zhou, S.; Lou, S. *Mater. Lett.* **2012**, *68*, 296−299.
(21) Huang, W. L.; Zhu, Q. *Comput. Mater. Sci.* **2009**, *46*, 1076−1084.
(22) Zhang, H.; Liu, L.; Zhou, Z. *Phys. Chem. Chem. Phys.* **2012**, *14*, 1286−1292.
(23) Li, T. B.; Chen, G.; Zhou, C.; Shen, Z. Y.; Jin, R. C.; Sun, J. X. *Dalton Trans.* **2011**, *40*, 6751−6758.
(24) Cao, J.; Xu, B.; Luo, B.; Lin, H.; Chen, S. *Catal. Commun.* **2011**, *13*, 63−68.
(25) Wang, W. D.; Huang, F. Q.; Lin, X. P. *Scr. Mater.* **2007**, *56*, 669−672.
(26) Shenawi-Khalil, S.; Uranov, V.; Kritsman, Y.; Menes, E.; Popov, I.; Sasson, Y. *Catal. Commun.* **2011**, *12*, 1136−1141.
(27) Liu, Y.; Son, W.-J.; Lu, J.; Huang, B.; Dai, Y.; Ehangbo, M.-H. *Chem.—Eur. J.* **2011**, *17*, 9342−9349.
(28) Huo, Y.; Zhang, J.; Miao, M.; Jin, Y. *Appl. Catal., B* **2012**, *111−112*, 334−341.
(29) Zhang, D.; Wen, M.; Jiang, B.; Li, G.; Yu, J. C. *J. Hazard. Mater.* **2012**, *211−212*, 104−111.
(30) Jiang, J.; Zhao, K.; Xiao, X.-Y.; Zhang, L.-Z. *J. Am. Chem. Soc.* **2012**, *134*, 4473−4476.
(31) Ye, L.; Zan, L.; Tian, L.; Peng, T.; Zhang, J. *Chem. Commun.* **2011**, *47*, 6951−6953.
(32) Chen, Y.; Wen, M.; Wu, Q. *CrystEngComm* **2011**, *12*, 3035−3039.
(33) Zhang, K.; Liang, J.; Wang, S.; Liu, J.; Ren, K.; Zheng, X.; Luo, H.; Peng, Y.; Zou, X.; Bo, X.; Li, J.; Yu, X. *Cryst. Growth Des.* **2012**, *12*, 793−803.
(34) Chang, X.; Gondal, M. A.; Al-Saadi, A. A.; Ali, M. A.; Shen, H.; Zhou, Q.; Zhang, J.; Du, M.; Liu, Y.; Ji, G. J. *Colloids Interface Sci.* **2012**, *377*, 291−298.
(35) Fox, M. A.; Dulay, M. T. *Chem. Rev.* **1993**, *93*, 341−357.
(36) Li, T. B.; Chen, G.; Zhou, C.; Shen, Z. Y.; Jin, R. C.; Sun, J. X. *Dalton Trans.* **2011**, *40*, 6751−6758.
(37) Herrmann, J.-M. *Appl. Catal., B* **2010**, *99*, 461−468.
(38) Yan, X.; Ohno, T.; Nishijima, K.; Abe, R.; Ohtani, B. *Chem. Phys. Lett.* **2006**, *429*, 606−610.
(39) Bahnemann, D. W. *Res. Chem. Intermed.* **2000**, *26*, 207−220.
(40) Maning, L. E.; Kramer, M. K.; Foote, M. K. *Tetrahedron Lett.* **1984**, *25*, 2523−2526.
(41) Ishibashi, K. *J. Photochem. Photobiol., A* **2000**, *134*, 139−142.
(42) Prairie, M. R.; Evans, L. R.; Stange, B. M.; Martinez, S. L. *Environ. Sci. Technol.* **1993**, *27*, 1776−1782.